Supplementary Information (SI) for Journal of Materials Chemistry A.
This journal is © The Royal Society of Chemistry 2026

Supplementary Information (SI) for

Facile Embedding of Aromatic Carbon Rings into g-C_3N_4 Framework for Boosting Piezocatalytic Water Splitting

Yingfeng Zhou,[a] Xiupeng Tang,[a] Jie Yuan,[b] Junhao Yang,[a] Peijun Yu,[a] Difa Xu,[a] Shiying Zhang,[a] Hui Wan*[a] and Wenhui Feng*[a]

[a] *Hunan Province Key Laboratory of Applied Environmental Photocatalysis, Changsha University, Changsha, 410022, P. R. China.*

[b] *State Key Laboratory of Photocatalysis on Energy and Environment, Fuzhou University, Fuzhou, 350116, P. R. China*

**Corresponding author.*

E-*mail addresses: fengwenhui1991@126.com* (W. Feng)*; huiwan@hnu.edu.cn* (H. Wan)

This PDF file includes:

Figure S1

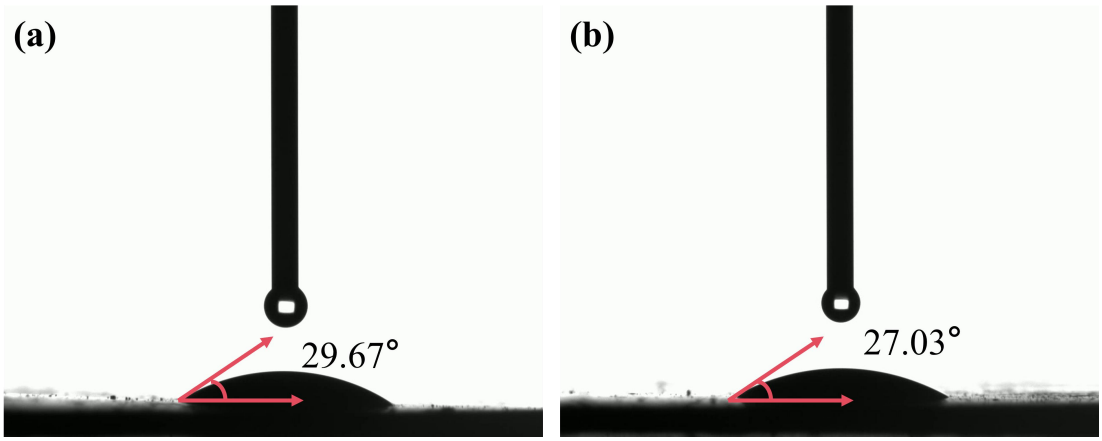

Fig. S1 Water contact angle measurements of (a) pure g-C_3N_4 and (b) optimal CNA_{40} sample.

Figure S2

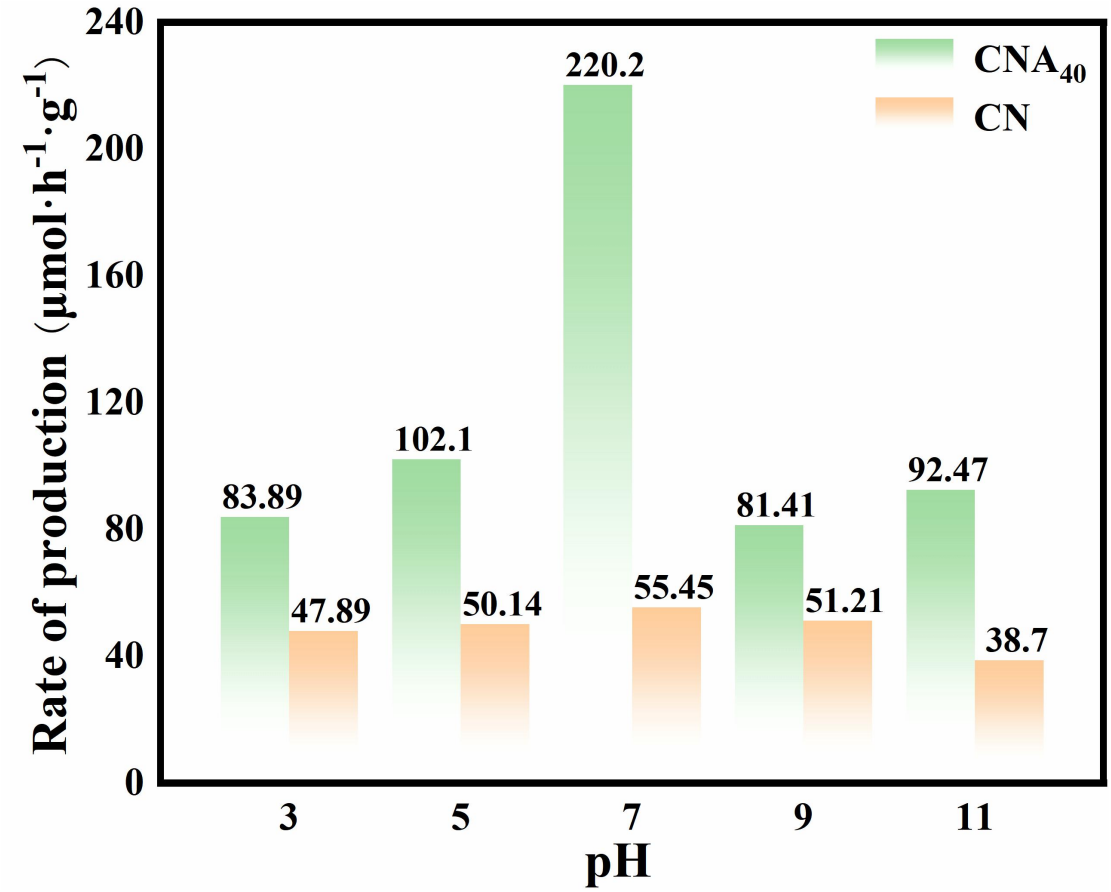

Fig. S2 Effect of solution pH on the piezocatalytic hydrogen production performance of CNA_{40} and CN catalysts.

Figure S3

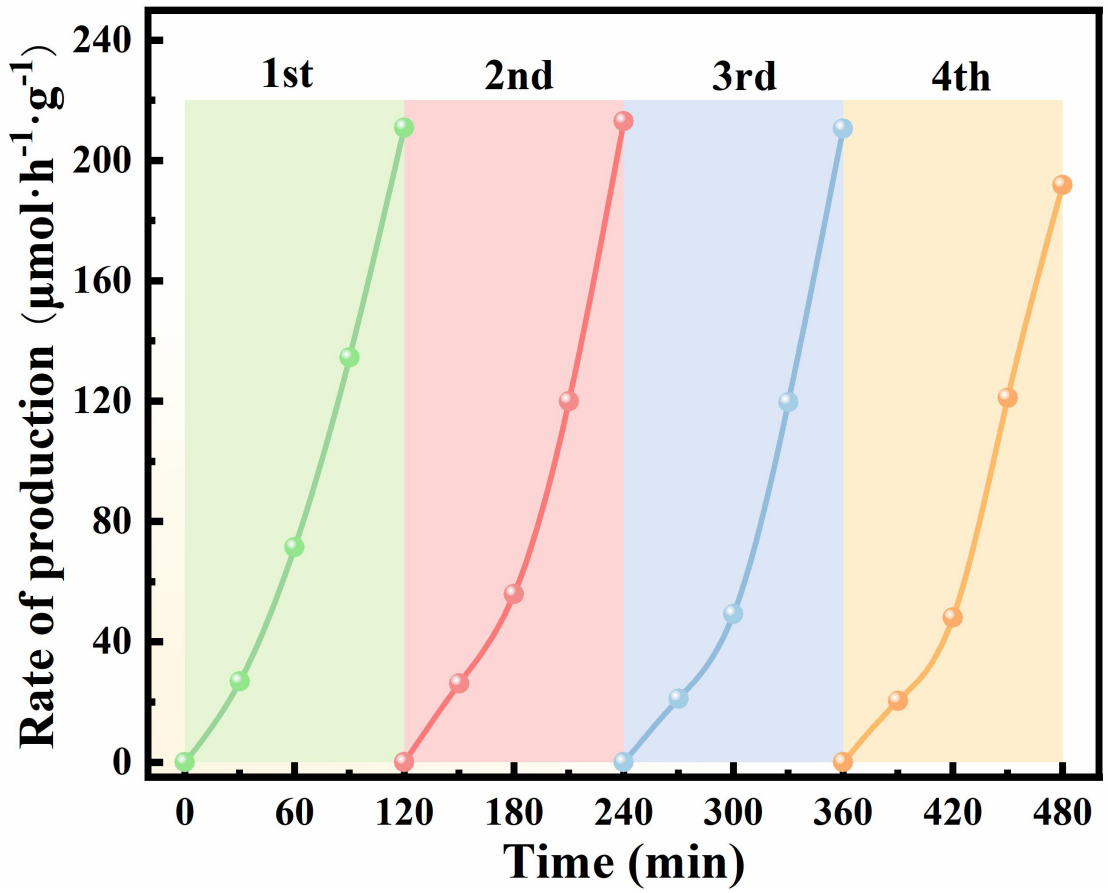

Fig. S3 Long-term cyclic piezocatalytic hydrogen evolution performance of CNA_{40} catalyst.

Figure S4

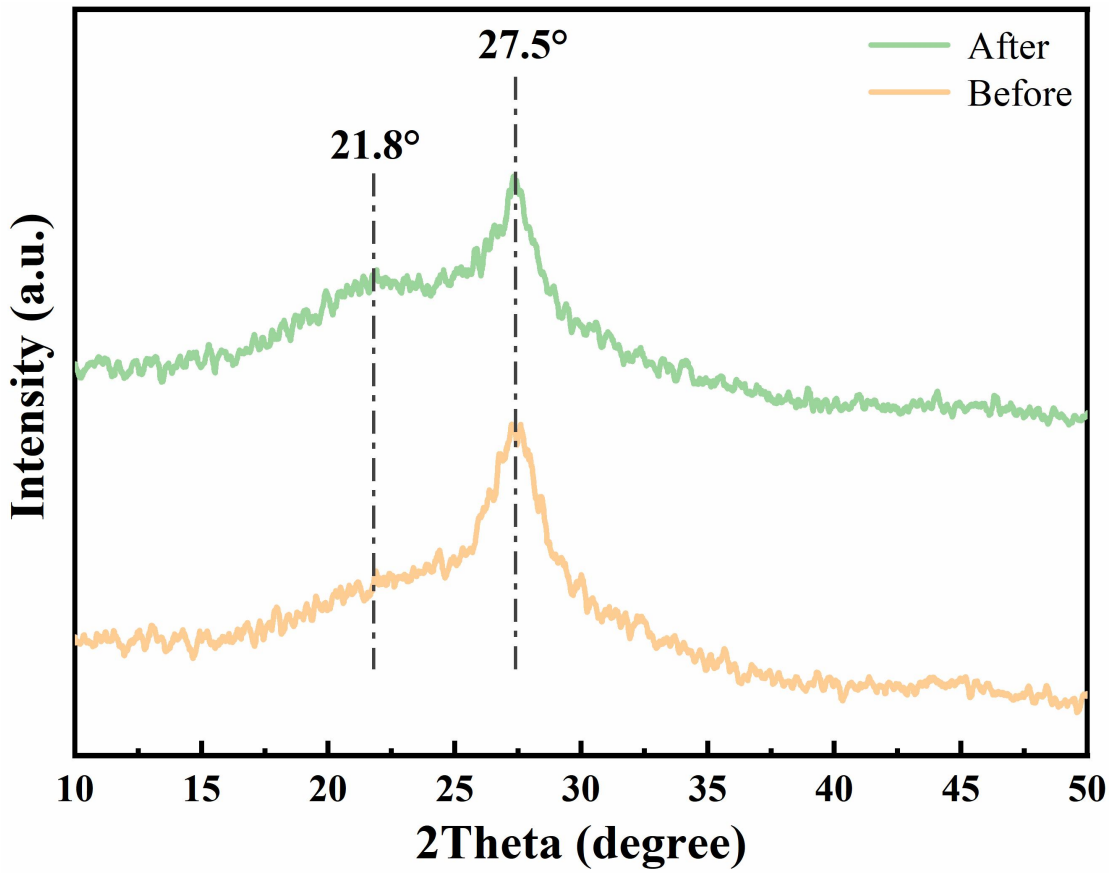

Fig. S4 Comparison of XRD patterns of CNA_{40} before and after piezocatalytic reaction.

Test were carried out on CNA_{40} after the fourth round of the cycle. As shown in the XRD patterns in Fig. S4, the characteristic diffraction peak positions of CNA_{40} remain completely unchanged before and after the reaction. This confirms that the intrinsic crystal framework of the material remains intact and no new phases are formed. A slight decrease in the intensity of the (002) peak at 27.5° is accompanied by a marginal reduction in crystallinity.

Figure S5

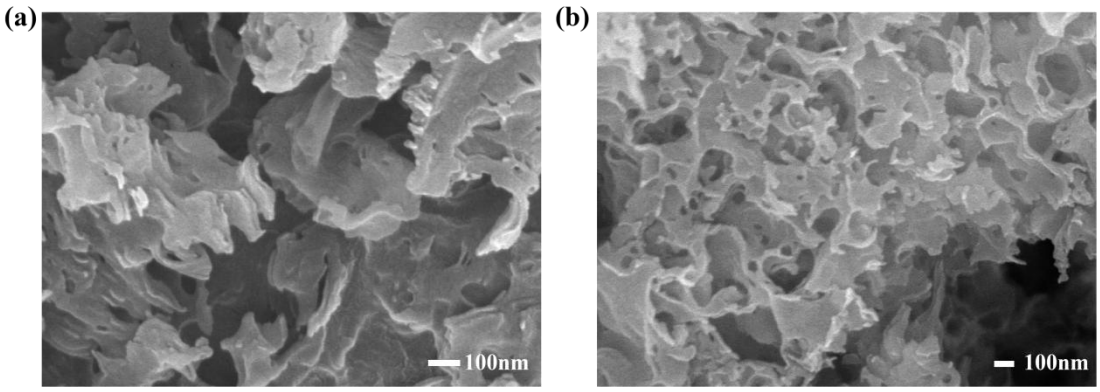

Fig. S5 SEM characterization of the morphology of CNA_{40} after piezocatalytic hydrogen evolution reaction.

Furthermore, the SEM images (Fig. S5) demonstrate that CNA_{40} retains its typical two-dimensional layered nanosheet structure before and after the reaction. No significant differences are observed in the morphology, size, or stacking state of the nanosheets, and no obvious agglomeration, fragmentation, or structural collapse is detected. After the reaction, the surface porosity of the nanosheets slightly increases. It is speculated that this is caused by mild adjustment under continuous mechanical stress during the piezocatalytic process, which does not affect the overall morphology of the material.

Calculation of energy conversion efficiency

The efficiency of converting mechanical energy to chemical energy is estimated by the ratio of the output chemical energy and the ultrasonic energy received by the reaction suspension. During the piezocatalytic reaction, the liquid level of the suspension in the reactor is kept equal to the external propagation medium (water) as illustrated in Scheme S1.[1]

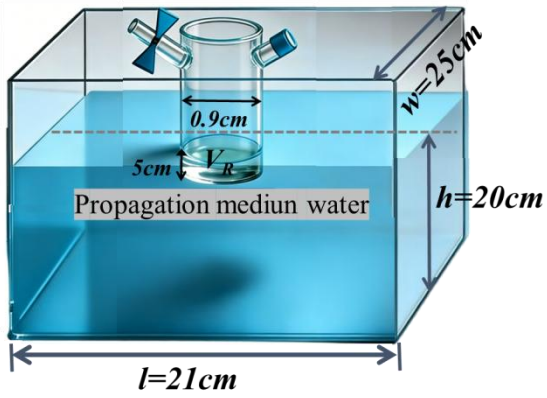

Scheme S1 Schematic diagram of piezocatalytic reaction unit.

The volume of the reactor immersed in propagation medium (water), V_R

$V_R = \pi*(5/2)^2*0.9\ cm^3 = 17.67\ cm^3$

The volume of propagation medium (water), V_0

$V_0 = lwh = 21*25*20\ cm^3 = 10500\ cm^3$

The ultrasonic power received by the reactor, I_R

$I_R = P_0*(V_R/V_0) = 100 * (17.67/ 10500)\ W = 0.1683\ W$

Where P_0 = ultrasonic power from the ultrasonic generator.

The reflectivity of glass tube against the ultrasonic vibrations, R

$$R = \left(\frac{\rho(\text{glass})c(\text{glass}) - \rho(\text{water})c(\text{water})}{\rho(\text{glass})c(\text{glass}) + \rho(\text{water})c(\text{water})}\right) = \left(\frac{2.8 * 2E8 - 1.0 * 2.25E8}{2.8 * 2E8 + 1.0 * 2.25E8}\right)$$

$$= 0.185$$

Where ρ = density of media; c = speed of light in media.

The ultrasonic energy received by the reaction suspension, E_{mech}

$E_{mech}=(1-R) * I_R * t = (1-0.185) * 0.1683 * 3600\ J = 493.7922\ J$

The output chemical energy, E_{chem}

$E_{chem}=2n_{H2}E_teN_A=2 * 4.26E(-6)(mol) * 1.23(eV) * 1.602E(-19) * 6.02E(23)=1.01\ J$

Where n_{H2} = hydrogen produced in moles; E_t = threshold energy of water decomposition =1.23 eV; N_A = Avogadro's number; e = electron volt.

The energy conversion efficiency of sample, η

$\eta = (E_{chem}/ E_{mech}) * 100\% = 0.2\%$

Table S1. Comparison of piezocatalytic H_2 production performance over typical piezocatalysts previous reported and aromatic carbon rings embedded in carbon nitride in this work.

Piezocatalysts	Catalytic Conditions	Sacrificial Agents	Multiplication factor	Catalytic Activity	Ref.
Aromatic carbon rings embedded in g-C_3N_4	Ultrasonic vibration (50 W, 40 KHz)	None	3.75	214.69 μmol·g^{-1}·h^{-1}	This Work
Tubular g-C_3N_4	Ultrasonic vibratio (160 W, 40 KHz)	1.4 mol/L glucose, 2 wt% Pt	2.7	2014.7 μmol·g^{-1}·h^{-1}	[2]
Carbon ring doped g-C_3N_4	Ultrasonic vibration (160 W, 40 KHz)	250 g/L glucose, 2 wt% Pt	2	1473.2 μmol·g^{-1}·h^{-1}	[3]
Nitrogen vacancy and Cl doping of g-C_3N_4	Ultrasonic vibration (160 W, 40 KHz)	250 g/L glucose, 2 wt% Pt	2.6	1961 μmol·g^{-1}·h^{-1}	[4]
Silver monatomic and cluster co-modified g-C_3N_4	No specific explanation provided	None	2.1	7.90 mmol·g^{-1}·h^{-1}	[5]
1T/2H flake-like MoS_2 / protonated g-C_3N_4	Ultrasonic vibration (150 W, 40 KHz)	10 vol% Triethanolamine	3.3	1070 μmol·g^{-1}·h^{-1}	[6]
g-C_3N_4/ZnO nanorods	Ultrasonic vibration (60 W, 40 KHz, 50 W visible light)	10 vol% methanol	1.81	1497.5 μmol·g^{-1}·h^{-1}	[7]
Sulfur vacancies control MoS_2	Ultrasonic vibration (80 W, 40 KHz)	MeOH	3.24	1423.29 μmol·g^{-1}·h^{-1}	[8]
O vacancies control MoS_2	Ultrasonic vibration (100 W, 40 KHz)	H_2O	2.36	47.75 μmol·g^{-1}·h^{-1}	[9]
Sn doped into $SrTiO_3$	Ultrasonic vibration (80 W, 40 KHz)	None	3.28	101.46 μmol·g^{-1}·h^{-1}	[10]
MoS_2@Mo_2CT_x	Ultrasonic vibration (300 W, 40 KHz)	MeOH	3.06	1164.8 μmol·g^{-1}·h^{-1}	[11]
MoS_2/ZnO/$CuFe_2O_4$ nanosheets	Magnetic stirring at 400 rpm	10 vol% methanol	2.19	3150 μmol·g^{-1}·h^{-1}	[12]

References

[1] W. Feng, J. Yuan, L. Zhang, W. Hu, Z. Wu, X. Wang, X. Huang, P. Liu and S. Zhang, *Appl. Catal. B: Environ.*, **2020**, 277, 119250.

[2] J. Nie, J. Guo, S. Liang, S. Li, H. Yu and C. Wu, *Chem. Commun.*, **2026**, 1359–1364.

[3] J. Nie, S. Yue, B. Li, J. Guo and C. Wu, *Ceram. Int.*, **2025**, 51, 31370–31377.

[4] K. Zhang, X. Sun, H. Hu, G. Yan, A. Qin, Y. Ma, H. Huang and T. Ma, *Small*, **2023**, 19, 6810–6829.

[5] C. Hu, J. Hu, Z. Zhu, Y. Lu, S. Chu, T. Ma, Y. Zhang and H. Huang, *Angewandte Chemie International Edition*, **2022**, 61, 12397.

[6] Y. Wang, H. Ma, J. Liu, Z. Zhang, Y. Yu and S. Zuo, *J. Colloid Interface Sci.*, **2024**, 665, 655–680.

[7] P. Gotipamul, R. Maheswaran, S. Pandiaraj, S. A. Alqarni and S. Chidambaram, *Mater. Today Sustain.*, **2023**, 24, 100501.

[8] S. Mondal, K. Dilly Rajan, L. Patra, M. Rathinam and V. Ganesh, *Small*, **2025**, 21.

[9] R. Lei, F. Gao, J. Yuan, C. Jiang, X. Fu, W. Feng and P. Liu, *Appl. Surf. Sci.*, **2022**, 576, 151851.

[10] Z. Chen, W. Liu, L. Zheng, Q. Chen, Y. Liu, S. Lan and M. Zhu, *Sep. Purif. Technol.*, **2025**, 353, 128307.

[11] H. Y. Lin and J. M. Wu, *Adv. Energy Mater.*, **2024**, 14, 02164.

[12] M. Lu and X. Wu, *ACS Appl. Nano Mater.*, **2025**, 8, 5078–5091.